International Journal of Geo-Information

MDPI

Article

Quantifying Long-Term Spatiotemporal Variation in and Drivers of the Surface Daytime Urban Heat Island Effect in Major Chinese Cities: Perspectives from Different Climate Zones

Minxue Zheng, Dianwei Zheng, Qiu Shen and Feng Jia *

Department of Environment and Safety & Engineering, Jiangsu University, Zhenjiang 212013, China; zmx@ujs.edu.cn (M.Z.); 2222309075@stmail.ujs.edu.cn (D.Z.); 1000006342@ujs.edu.cn (Q.S.)
* Correspondence: fjia@ujs.edu.cn

Abstract

The urban heat island (UHI) effect and its associated extreme weather events have adverse impacts on human environment-coupled systems. However, the spatiotemporal variations in the UHI effect, as well as potential influencing factors, across climate zones remain poorly understood. This study explored how climate zones influenced the spatiotemporal variation in, trends in, and drivers of summer daytime surface UHI intensity (SUHII) in 220 Chinese cities located in five climate zones from 2000 to 2020. SUHII was quantified using MODIS land surface temperature (LST) data and remote sensing-derived urban built-up area masks were used to quantify SUHII. The Mann–Kendall test was applied to detect long-term SUHII trends, while Pearson correlation and stepwise multiple regression analyses were performed to identify key climatic and geographic drivers across different climate zones. The results indicated summer daytime SUHII values of 1.75 °C ± 1.19 °C, 1.74 °C ± 0.81 °C, 2.37 °C ± 0.75 °C, 2.14 °C ± 1.00 °C, and 2.36 °C ± 0.91 °C for the middle temperate zone (MTZ), south temperate zone (STZ), north subtropical zone (NSZ), middle subtropical zone (MSZ), and south subtropical zone (SSZ), respectively. In most cities, the SUHII increased significantly over time ($p < 0.05$). Pearson's correlation analysis indicated that the enhanced vegetation index (EVI) and net radiation (NR) were moderately correlated with the SUHII in the MTZ, with correlation coefficients (r) of 0.465 and 0.42 ($p < 0.05$). Using a multivariate stepwise regression model, the relative contributions of various influencing factors to the UHI effect were quantified, explaining 27.1% to 57.2% of the variation across different climate zones. In particular, the economic vulnerability index and population density were the main factors affecting the SUHII in the MTZ and SSZ. Our findings support the development of policies aimed at mitigating the UHI effect by addressing the specific requirements of different climate zones to reduce.

Keywords: urban heat island; climate zone; spatiotemporal characteristics; driving factors; stepwise multiple linear regression model

check for updates

Academic Editors: Wolfgang Kainz and Godwin Yeboah

Received: 14 March 2025
Revised: 7 June 2025
Accepted: 20 June 2025
Published: 23 June 2025

Citation: Zheng, M.; Zheng, D.; Shen, Q.; Jia, F. Quantifying Long-Term Spatiotemporal Variation in and Drivers of the Surface Daytime Urban Heat Island Effect in Major Chinese Cities: Perspectives from Different Climate Zones. *ISPRS Int. J. Geo-Inf.* **2025**, *14*, 239. https://doi.org/10.3390/ijgi14070239

Copyright: © 2025 by the authors. Published by MDPI on behalf of the International Society for Photogrammetry and Remote Sensing. Licensee MDPI, Basel, Switzerland. This article is an open access article distributed under the terms and conditions of the Creative Commons Attribution (CC BY) license (https://creativecommons.org/licenses/by/4.0/).

1. Introduction

The urban heat island (UHI) effect is a well-documented urban climate phenomenon in which urban areas exhibit higher temperatures than their surrounding rural counterparts due to land surface modification and anthropogenic heat emissions [1,2]. UHIs are commonly categorized into Surface UHIs (SUHIs) and Atmospheric UHIs (AUHIs). SUHIs refer to surface temperature differences, typically measured by remote sensing-based land

surface temperature (LST), while AUHIs involve air temperature differences at near-surface levels. This study focuses on summer daytime SUHIs, which are strongly linked to heat stress and public health risk [3].

In recent years, the temporal dynamics and long-term persistence of SUHIs have received increasing attention. For instance, Stewart et al. (2021) [4] comprehensively quantified the time evolution of SUHI intensity and emphasized its dependence on urban morphology and surface energy balance. Moreover, recent studies suggest that under extreme heat, humid heat stress may exceed human physiological tolerance, lead to in heat-related mortality [5]. The interaction between extreme heatwaves and urban areas is a growing concern, as climate change is expected to increase the frequency and intensity of such events, further exacerbating urban temperatures. While researchers have investigated various spatiotemporal characteristics and drivers, significant gaps remain in understanding these dynamics. Further research is required to explore the spatiotemporal variations, trends, and influencing factors of the UHI effect in major cities worldwide [6,7].

Many researchers have used meteorological and remote sensing data to conduct extensive studies at the city and regional levels, drawing meaningful conclusions and achieving a broad consensus. Yao et al. (2017) [8] examined various spatiotemporal characteristics and discovered that surface UHI intensity (SUHII) in most Chinese cities was significantly higher during the summer daytime than in winter. Similarly, Imhoff et al. (2010) [9] found that most cities experienced greater SUHII variations and higher intensities during the summer daytime compared to other seasons. A major upward trend in SUHII has been observed in many cities, including increases in summer daytime SUHII over recent years in Italian cities [10], over the past 20 years in 20 major cities across India and neighboring countries [11], and throughout China [12]. In addition, an intrinsic link has been identified between the summer daytime UHI effect and extreme heat-wave events. For example, Ramamurthy et al. (2016) [13] reported variations in the interaction between multiple similarly sized cities and heat waves, noting that UHI–heatwave interaction patterns are often interconnected across cities.

Identifying factors that influence the SUHII is a prerequisite for its mitigation. These factors can be divided into three types: biophysical characteristics (e.g., city-and-ecological landscape ratio), natural factors (e.g., topography and soil moisture evaporation), and socioeconomic factors (e.g., population density and nighttime lighting) [14–19] In China, land use types and urban surfaces significantly influence the UHI effect [20,21], with anthropogenic heat release being a key driver of increased SUHII in urbanized areas [8,22]. Lu et al. (2025) [23] have highlighted how urban morphological characteristics influence heat accumulation, air circulation, and thermal dissipation, thereby modulating the intensity of the urban heat island effect. Similarly, Aslani et al. (2025) [24] identified population density, AOD, and built-up density as key UHI drivers in Tehran using multi-model analysis, reinforcing the need for region-specific mitigation frameworks. Despite these insights, most studies have focused on a limited number of influencing factors, which restrict our understanding of the impacts of the UHI effect [25,26].

Climate zones are increasingly recognized as critical in influencing UHI effects. For example, Lefevre et al. (2025) [27] explored UHI intensity differences of up to 4.14 °C on Réunion Island, demonstrating strong climatic zone–urban form interactions, thereby underscoring the value of zone-specific planning interventions. Although the influence of climate zones on UHI has gained attention, few comparative studies have explored their role in shaping UHI changes, trends, and drivers [25,28]. Kim et al. (2018) [29] quantified the UHI effect across U.S. a climate zones to determine the effectiveness of UHI mitigation strategies, which Mohammad et al. (2021) [30] reported that vegetation activity and evapotranspiration drive various spatiotemporal trends in the UHI effect across cities

in different climate zones. A comparison of SUHII between temperate and hot desert climate zones revealed that desert climates have a regulating or cooling effect whereas temperate cities experience the highest SUHII during summer [31]. However, several key gaps in research on the UHI effect remain. As highlighted by Li et al. (2022) [32], UHI intensity measurements across over 1000 global cities show large uncertainties due to inconsistent reference areas and cloud contamination in satellite data, underscoring the need for cautious interpretation and enhanced methodological rigor. For example, many studies are limited by short study periods, low data precision, narrow research scopes, and insufficient consideration of the influencing factors. Given the complexity of human–environment-coupled systems, conducting long-term, high-precision, and large-scale spatiotemporal studies from a climate zone perspective remains a major research priority. Quantifying the factors driving changes in UHIs is essential.

Climate change and rapid urbanization have significantly intensified the urban heat island (UHI) effect across Chinese cities, creating growing threats to urban thermal environments and public health. However, existing studies on the long-term spatiotemporal characteristics of urban thermal environments and their dominant drivers remain inadequate—particularly in quantifying the variations across different climate zones and elucidating their underlying mechanisms. To address these research gaps, this study aims to provide a long-term (21-year) quantitative analysis of urban heat island intensity on a national scale using consistent remote sensing datasets; introduce a climate zone-based perspective to compare SUHII dynamics across different environmental con-texts; and introduce a novel approach by conducting a large-scale attribution analysis across 220 cities from the perspective of climatic regionalization. This climate zone-based comparative framework not only enhances the spatial representativeness of UHI research but also provides tailored insights and mitigation strategies adapted to the specific biophysical and socioeconomic contexts of each climate zone. These findings offer new insights into the climatic regulation of urban heat risk and serve as a reference for climate-sensitive urban planning and heat mitigation policies. Specifically, the aims are to (1) evaluate a long-term (21-year) spatiotemporal characteristics of and trends in the UHI effect during summer in different climate zones and cities from 2000 to 2020; (2) determine the relative importance of various factors influencing SUHII; (3) offer specific recommendations for mitigating the UHI effect from a climate zone perspective. Collectively, our findings support the development of policies aimed at mitigating the UHI effect, reducing weather events associated with the UHI effect in different climatic zones, and promoting urban planning and ecological conservation.

2. Materials and Methods

2.1. Study Area

The UHI effect is a major environmental issue in China. Given that China has many climate zones, additional research on the spatiotemporal characteristics and influencing factors specific to each zone is necessary to effectively mitigate the UHI problem. This study adopted the climatic regionalization defined by the China Meteorological Administration, as it comprehensively reflects the country's varied climatic conditions (Supplementary Figure S1) [33]. To minimize geographic uncertainties, we excluded the northern temperate, plateau climate, northern tropical, and middle tropical zones, which are either sparsely populated or cover very small areas. Finally, we selected 220 cities with areas exceeding 10 km^2, accounting for 75.09% of all cities in China. These included 50 cities in the middle temperate zone (MTZ), 67 in the southern temperate zone (STZ), 37 in the northern subtropical zone (NSZ), 45 in the middle subtropical zone (MSZ), and 21 in the southern subtropical zone (SSZ) (Figure 1).

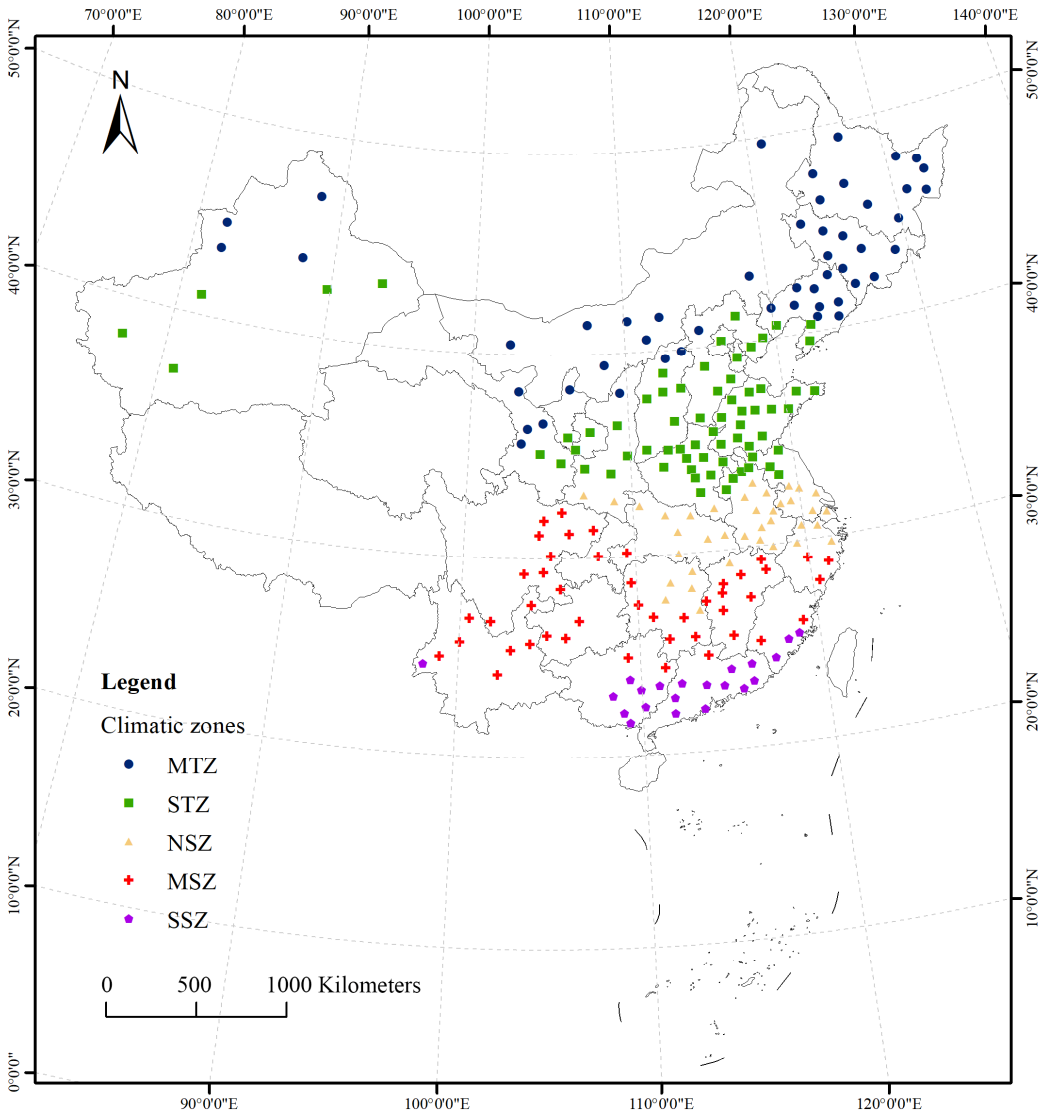


Figure 1. Locations of the 220 sampled cities in China, including 50 cities in the middle temperate zone (MTZ), 67 in the south temperate zone (STZ), 37 in the north subtropical zone (NSZ), 45 in the middle subtropical zone (MSZ), and 21 in the south subtropical zone (SSZ).

2.2. Data Sources

Terra MODIS (MOD11A2, version 6) 8-day composite (Level 3) 1000 m land surface temperature (LST) products were used. These products are widely utilized in UHI research due to their extended series, global coverage, and high accuracy. The LST products from 2000 to 2020 were retrieved from the MODIS website (https://ladsweb.modaps.eosdis.nasa.gov/). Summer daytime composite LST products (June to August, local solar time 13:30) for 2000–2020 were processed using the MODIS Reprojection Tool and ArcGIS [34,35]. To minimize cloud interference, only datasets with less than 5% cloud cover were used for analysis, and missing values were addressed by averaging the LST products [36]. Based on the scaling factor, the LST data (°C) were calculated using Equation (1).

$$LST = DN \times 0.02 - 273.15 \quad (1)$$

where DN is the pixel value of the MOD11A2 product [4,37,38].

Surface urban heat island intensity (SUHII) is defined as the difference in mean land surface temperature (LST) between urban built-up areas and their surrounding suburban regions, following the classical framework by Oke (1982), Voogt & Oke (2003), and Stewart

(2021) [1,4,39]. Compared to administrative boundaries, urban built-up areas more effectively capture the biophysical characteristics of cities [4,40]. Thus, we utilized the global annual urban extents dataset (1992–2020) derived from harmonized nighttime lights to delineate urban areas [41]. This dataset provides a consistent historical record of urbanization and its high accuracy has been validated in previous studies [42]. Suburban areas were defined as equal-area buffer zones surrounding urban built-up areas, generated using spatial analysis tools in Python 3.10 [43,44]. To minimize measurement biases, pixels containing water bodies or other urban clusters within suburban buffers were excluded [45,46].

To comprehensively examine the relationship between various potential influencing factors and changes in SUHII, 17 relevant factors were selected based on studies primarily examining UHI intensity [14,44,47,48]. The years 2001, 2005, 2010, 2015, and 2018 were selected for the attribution analysis of the SUHII using a multiple stepwise regression model considering the availability of multisource data (Table 1). Importantly, the land use/land cover data and other driving variables used in each selected year correspond exactly to the same that year's MODIS land surface temperature (LST) data, ensuring year-by-year temporal alignment. This methodological consistency minimized temporal mismatches between explanatory and response variables, allowing for a more accurate interpretation of SUHII dynamics in relation to urban expansion, greenness, climate, and human activity. These specific years were also chosen because they represent key stages in China's urbanization trajectory, making the analysis more policy-relevant and reflective of long-term trends.

Table 1. Potential drivers used in this study (2001, 2005, 2010, 2015, and 2018).

Categories	Factors (Abbreviation)	Description
Biophysical characters	Enhanced Vegetation Index (EVI)	Extracts the vegetation information of specific cities
	Landscape Shape Index (LSI)	Illustrates the complexity of urban shapes
	Percentage of Ecological Landscape (ECO)	/
	Percentage of Water Area (WAT)	/
	Percentage of Forest Area (FOR)	Reflects the biophysical characteristics of the city
	City area (City)	Major urban built-up areas
	Evapotranspiration (EVA)	Consumption of latent heat fluxes, including soil evaporation and vegetation transpiration
	Percentage of Impervious Surface (IMP)	/
	Percentage of Cropland (CRO)	/
	Percentage of Ecological proportion and Cropland (ECR)	/
Natural factors	Aerosol Optical Depth (AOD)	Longwave radiative forcing due to AOD strengthen the UHI
	Elevation (DEM)	/
	Net Radiation (NR)	Characterizes the surface radiation budget
	Precipitation (PRE)	/
Social–economic factors	Gross Domestic Product (GDP)	/
	Population density (POP)	/
	Nighttime Light (NL)	/

2.3. Methods

2.3.1. SUHII Definition

SUHII represents the difference in LST between urban and suburban areas. We used an island intensity index to quantitatively evaluate the spatiotemporal variation in the UHI effect. Specifically, SUHII was calculated as the average LST of the built-up area minus the average LST of an equal-area buffer zone in a suburban area [1,36,40] using Equation (2):

$$SUHII = LST_{urban} - LST_{rural} \quad (2)$$

where LST_{urban} is the average LST of the built-up area and LST_{rural} is the average LST of the equal-area buffer zone.

2.3.2. Statistical Analysis

The Mann–Kendall test was used as a nonparametric statistical method. This test does not rely on any specific data distribution and is not influenced by minor outliers, making it suitable for analyzing trends in the summer daytime SUHII [12,49]. To explore the correlation between potential influencing factors and the UHI effect, Pearson's correlation analysis was conducted to determine the significance of each factor. Multiple stepwise regression was then performed to quantify the relative contribution of each key factor to UHI variation [50].

The flow chart of this study is shown in Figure 2.

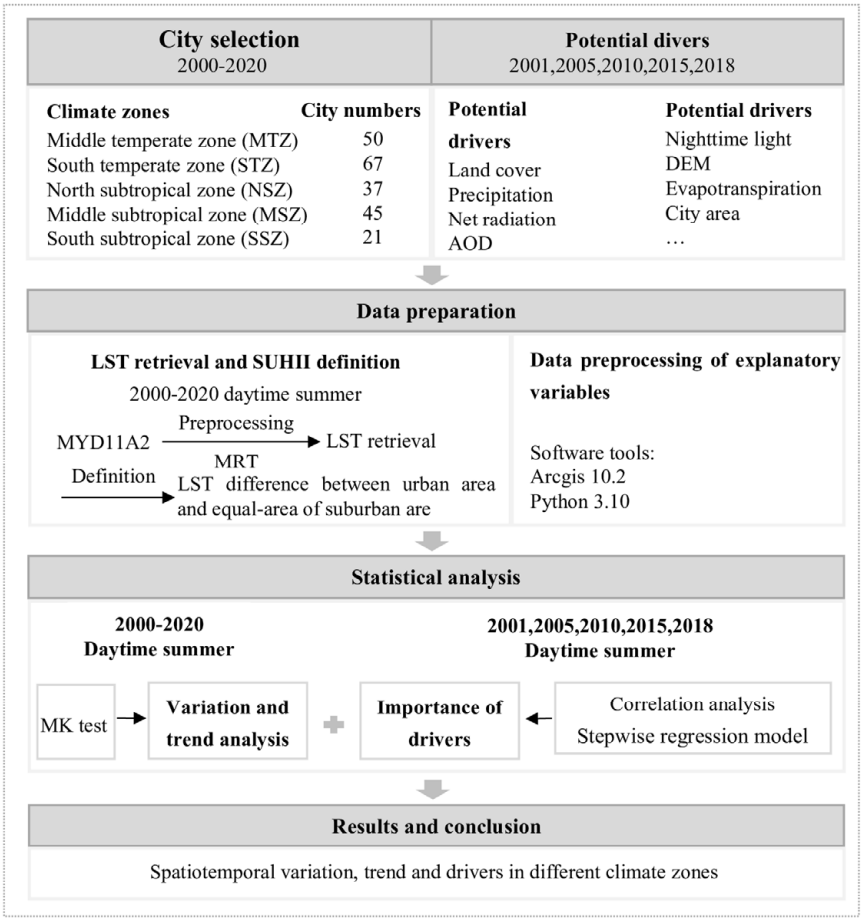


Figure 2. Flow chart of this study. MRT, LST, MK test, and AOD are abbreviations of MODIS reprojection tool, land surface temperature, Mann–Kendall test, and aerosol optical depth.

3. Results

3.1. SUHII Distribution

Figure 3 illustrates the distribution of the summer daytime SUHII in all cities from north to south between 2000 and 2020. During summer, the SUHII exhibited major spatiotemporal variations, indicating distinct climatic heterogeneity. The highest SUHII of 5.55 °C was recorded in Kunming in 2016, whereas the lowest SUHII of −2.59 °C was recorded in Alxa League in 2020. The average summer daytime SUHII values for the MTZ, STZ, NSZ, MSZ, and SSZ were 1.75 °C ± 1.19 °C, 1.74 °C ± 0.81 °C, 2.37 °C ± 0.75 °C, 2.14 °C ± 1.00 °C, and 2.36 °C ± 0.91 °C, respectively.

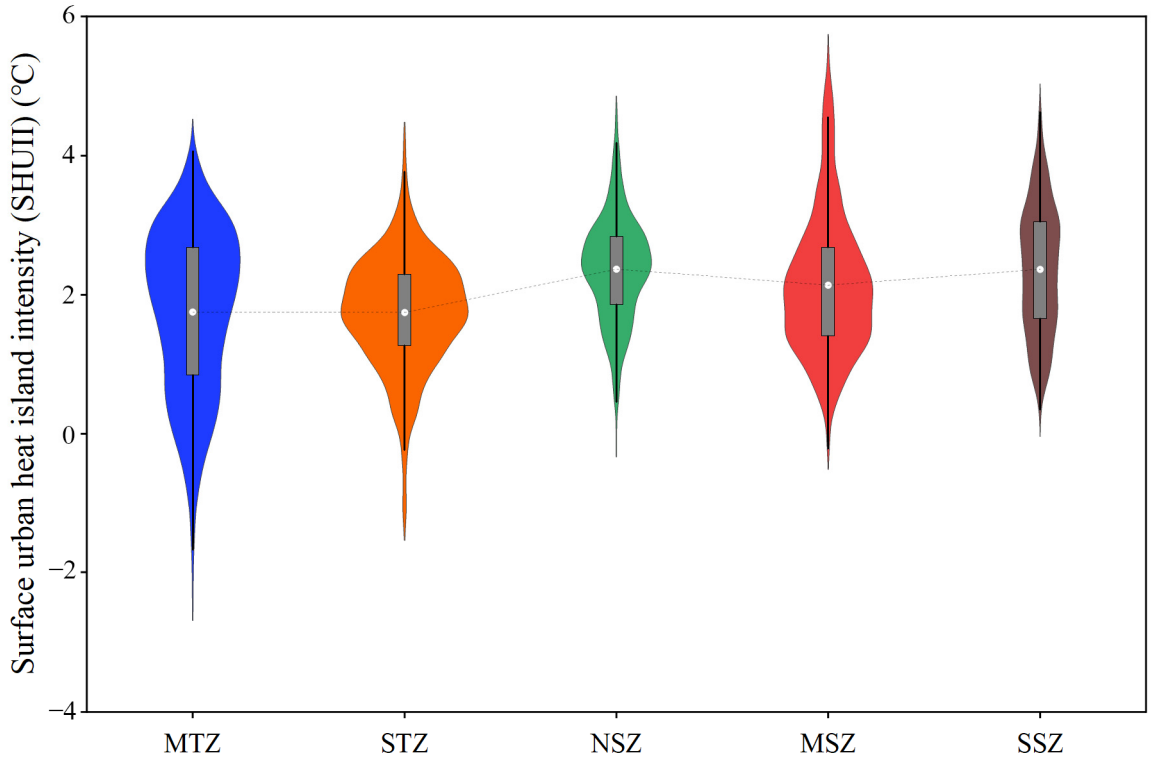


Figure 3. Distribution of surface urban heat island intensity (SUHII) in 220 cities across five climate zones.

To provide a more detailed understanding of SUHII variation across different climate zones, we further compared representative cities within each zone. In the NSZ, cities such as Wuhan and Changsha showed relatively high SUHII values, reaching up to 4.5 °C in peak years, possibly due to high population density and low vegetation coverage. In contrast, cities such as Nanning exhibited lower SUHII values, potentially attributed to higher rainfall and evapotranspiration rates. In the STZ, cities such as Jinan and Zhengzhou consistently ranked among the highest in SUHII, showing clear increasing trends over the past two decades. Meanwhile, cities in the middle temperate zone, such as Hohhot and Urumqi, generally showed lower SUHII values, likely due to lower background temperatures and smaller built-up extents. These spatial contrasts indicate that even within the same climate zone, urban form, vegetation, and socioeconomic factors can lead to substantial differences in heat island effects.

3.2. Temporal Trends in SUHII

From 2000 to 2020, the trend in summer daytime SUHII was significant in all cities ($p < 0.05$; Figure 4). In most cities, the surface UHI effect exhibited an upward trend, with climate zones exerting a particularly strong effect on the summer daytime SUHII. An analysis of summer daytime SUHII trends in cities across various climate zones (Figure 5) indicated that, in addition to cities located in the MTZ and STZ, more than 60% of cities in the NSZ, MSZ, and SSZ exhibited an increasing SUHII trend. In contrast, in the STZ and NSZ, the proportions of cities with an insignificant increasing trend and an insignificant decreasing trend were nearly identical. However, in the MTZ, MSZ, and SSZ regions, the proportion of cities with an insignificant increasing trend was significantly higher than that with an insignificant decreasing trend. Overall, the summer daytime SUHII exhibited an upward trend in 75.90% of cities. Spatially, high-SUHII clusters emerged in Central–Eastern China, particularly in the Yangtze River Basin and parts of the North China Plain. These patterns suggest a growing disparity in urban thermal stress across regions, indicating that heat exposure is becoming increasingly concentrated in more densely populated and rapidly developing urban clusters.

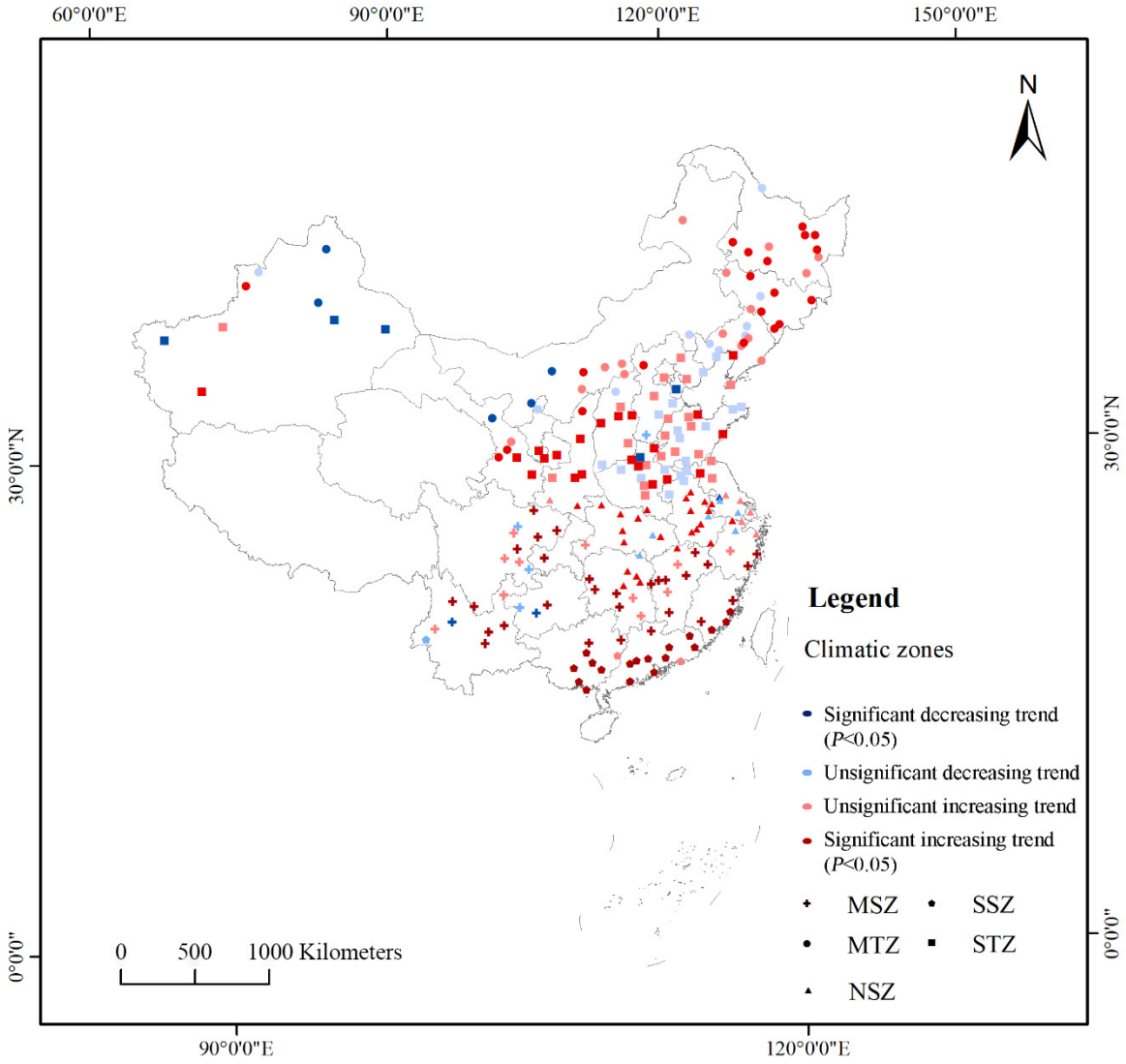


Figure 4. Temporal trends of summer daytime surface urban heat island intensity (SUHII) in 220 cities from 2000 to 2020.

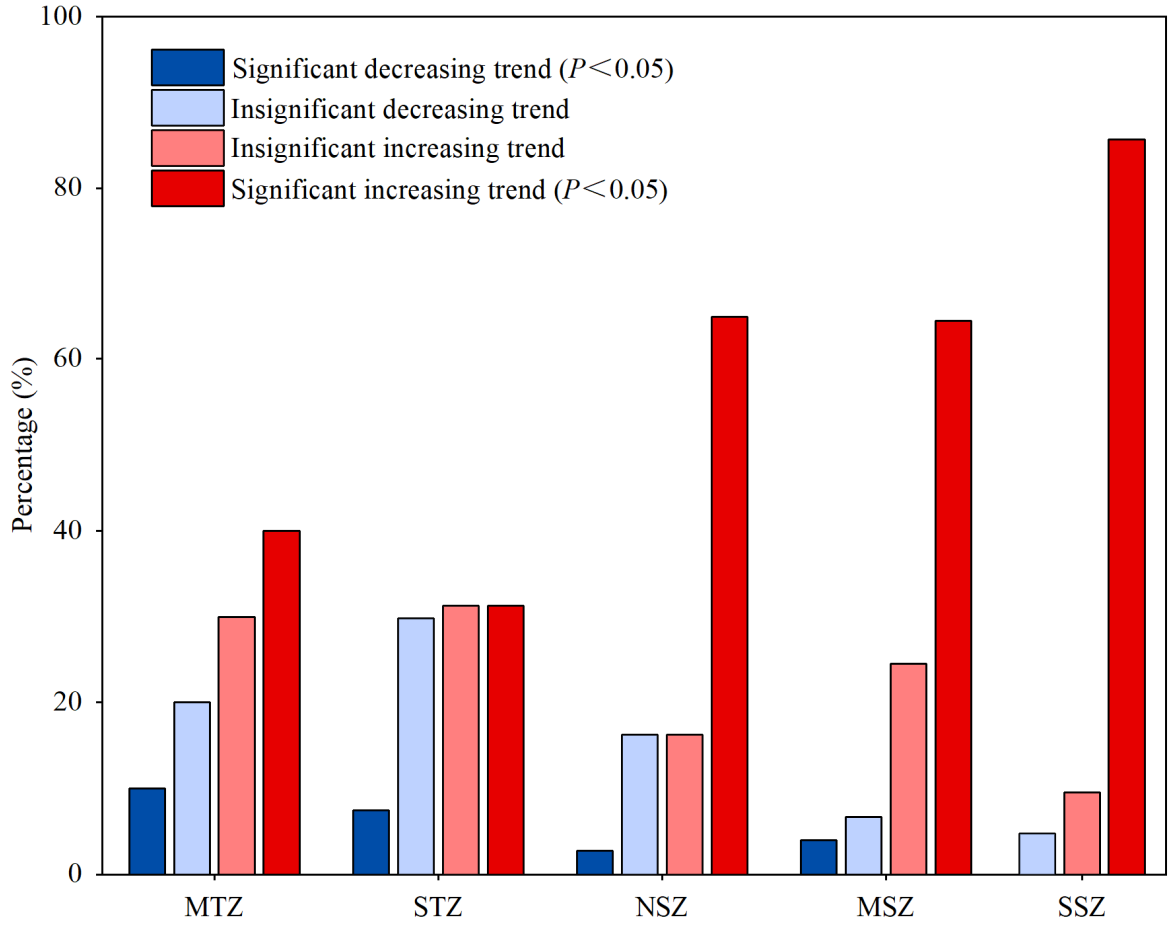


Figure 5. Trends in urban surface heat island effect as a percentage of summer daytime surface urban heat island (SUHII) effect in 220 cities across five climate zones.

3.3. Correlation Analysis of SUHII and Its Potential Drivers

We used data from 17 factors covering the years 2001, 2005, 2010, 2015, and 2018 to conduct Pearson's correlation and multiple stepwise regression analyses. Pearson's correlation analysis was conducted to evaluate the impacts of various factors on the UHI effect across the five climate zones ($p < 0.05$; Figure 6). In the temperate regions (MTZ and STZ), SUHII exhibited a significant negative correlation with DEM and a significant positive correlation with AOD. This finding suggests that both elevation and aerosol concentration are key factors regulating land surface temperature. Specifically, in relatively arid areas, increasing elevation can naturally suppress the urban heat island effect, while aerosols act as an insulating layer by reducing the dissipation of surface heat, thereby intensifying the heat island phenomenon. In the subtropical zones (NSZ, MSZ, SSZ), AOD and PRE emerged as important natural factors with moderate correlations to SUHII. AOD was negative correlated with SUHII in most subtropical cities, possibly reflecting the combined effects of reduced surface radiation and enhanced atmospheric trapping. Precipitation was generally negatively correlated with SUHII, implying a cooling influence mediated by surface moisture and evapotranspiration. Socioeconomic variables such as GDP and nighttime light (NL) showed strong but inconsistent correlations with SUHII across most zones. This pattern may be due to their indirect effects, acting through biophysical changes such as increased impervious surfaces or anthropogenic heat emissions.

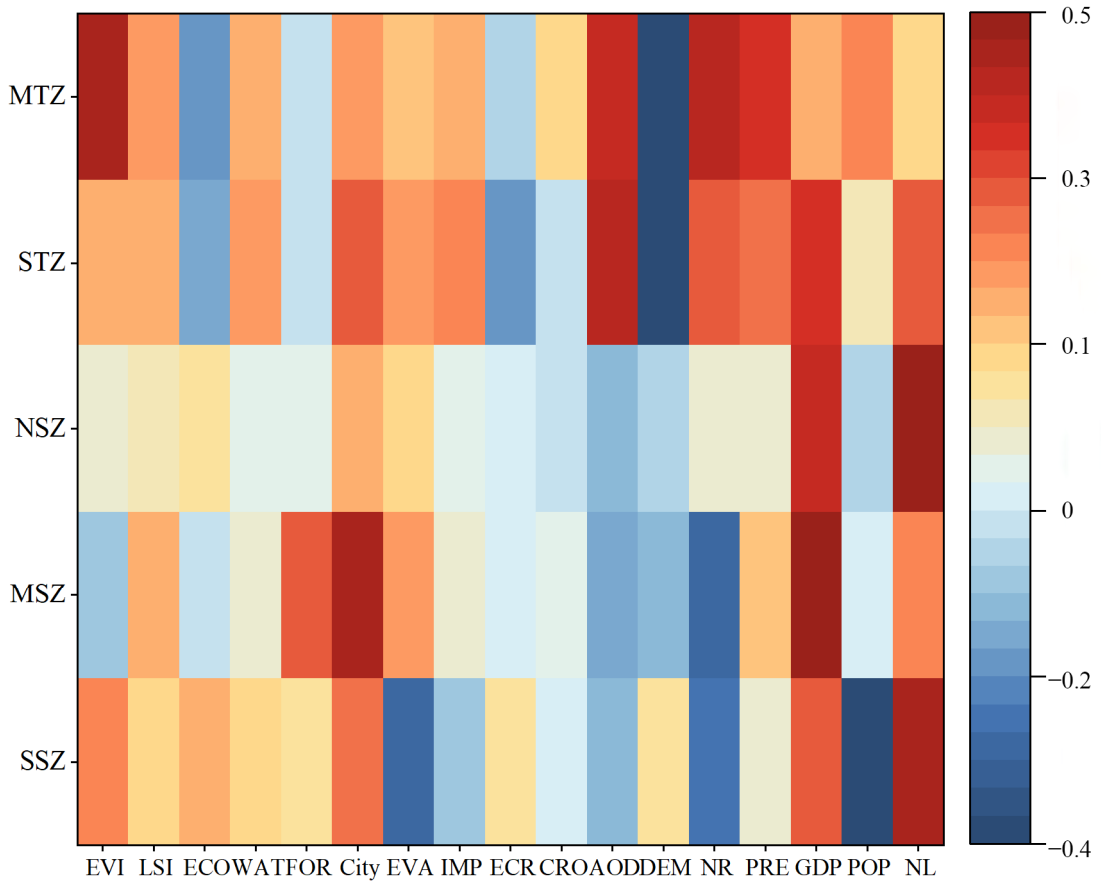


Figure 6. Correlation analysis of potential factors with SUHII.

3.4. Determination of the Dominant Factors Influencing SUHII

After identifying the factors influencing SUHII in all cities, a multiple stepwise regression analysis was conducted. As listed in Table 2, the relative contributions of the prediction models reflect the contributions of various factors to the UHI effect. When accounting for the different influencing factors, the five regression models explained 39.1%, 36.9%, 27.1%, 40.8%, and 57.2% of the SUHII variation in the MTZ, STZ, NSZ, MSZ, and SSZ, respectively. The analysis revealed that key SUHII drivers vary significantly by climate type, supporting the hypothesis of climatic heterogeneity in UHI formation. In the MTZ and STZ, the most influential factors were EVI, City, and IMP, with EVI alone explaining up to 48.78% of the variance in SUHII in the MTZ. This finding indicates that vegetation loss and the expansion of built-up areas are the dominant mechanisms contributing to surface heating in temperate cities, where natural cooling from EVA is relatively limited. In contrast, in the NSZ, MSZ, and SSZ, natural factors such as AOD and precipitation were the primary contributors. For example, AOD and PRE jointly accounted for more than 40% of the variation in SUHII in the SSZ and MSZ, emphasizing the atmospheric regulation of surface heat in these humid and monsoon-affected zones. Although socioeconomic factors such as GDP and population were included in the models, they emerged as moderate significant predictors. This finding suggests that their influence is likely indirect, operating through changes in land cover, anthropogenic emissions, and urban morphology, rather than directly driving surface temperature differences.

Table 2. Regression results for five different climate zones with the impact factor as the predictor variable and UHI intensity as the response variable. "Std. error" represents the standard error. "DW" refers to the Durbin–Watson test; a "DW" value close to 2 indicates that there is no first-order autocorrelation in the model.

Climate Zone	Factors	Unstandardized Coefficients		Standardized Coefficients	t	*p*-Value	Relative Contribution (%)	Regression Model	R^2	Adjusted R^2	F ($p < 0.01$)	DW
		B	Std. Error	Beta								
MTZ	(Constant)	−2.125	0.329	/	−6.450	0.000	/	UHI = 0.001 EVI + 0.002 City − 2.125	0.391	0.382	15.428	1.976
	EVI	0.001	0.000	0.554	10.066	0.000	48.780					
	POP	0.000	0.000	0.372	6.761	0.000	32.680					
	City	0.002	0.000	0.210	3.928	0.000	18.540					
STZ	(Constant)	2.790	0.797	/	3.501	0.001	/	UHI = 1.007 AOD + 0.038 NL − 0.113 NR + 0.033 EVA + 8.982 WAT + 2.790	0.369	0.353	4.090	1.880
	AOD	1.007	0.139	0.429	7.233	0.000	26.600					
	NL	0.038	0.007	0.273	5.105	0.000	16.920					
	GDP	0.000	0.000	0.193	3.596	0.000	11.960					
	PRE	0.000	0.000	0.218	3.348	0.001	13.510					
	Others	/	/	/	/	<0.05	30.990					
NSZ	(Constant)	1.777	0.113	/	15.690	0.000	/	UHI = 0.047 NL + 1.777	0.271	0.261	4.464	2.131
	NL	0.047	0.010	0.401	4.693	0.000	68.890					
	GDP	0.000	0.000	0.181	2.113	0.036	31.110					
MSZ	(Constant)	2.484	0.247	/	10.040	0.000	/	UHI = 12.331 FOR + 0.002 City − 1.883 ECR − 0.241 LSI + 0.081 EVA + 2.484	0.408	0.390	5.462	2.206
	GDP	0.000	0.000	0.248	3.497	0.001	15.550					
	FOR	12.331	2.199	0.351	5.608	0.000	22.000					
	City	0.002	0.000	0.414	4.758	0.000	25.960					
	ECR	−1.883	0.511	−0.232	−3.686	0.000	14.540					
	Others	/	/	/	/	<0.05	21.950					
SSZ	(Constant)	2.862	0.862	/	3.322	0.001	/	UHI = 0.079 NL − 0.059 EVA + 0.001 EVL − 1.901 IMP − 2.985 AOD + 2.862	0.572	0.543	8.164	1.697
	NL	0.079	0.011	0.522	7.234	0.000	26.550					
	EVA	−0.059	0.009	−0.490	−6.393	0.000	24.920					
	EVL	0.001	0.000	0.279	3.906	0.000	14.190					
	IMP	−1.901	0.632	−0.238	−3.008	0.003	12.110					
	Others	/	/	/	/	<0.05	22.210					

4. Discussion

4.1. Spatiotemporal Characteristics of SUHII

The UHI effect exhibits distinct spatiotemporal characteristics, and its intensity often varies by season, time of day, and geographic context. Our findings confirm that summer daytime SUHII is more pronounced than in other seasons, aligning with the findings of Montaner et al. (2020) [51] in Santiago and Li et al. (2017) [52] in the United States. However, by incorporating climate zone differentiation, our study provides a more nuanced spatial understanding of UHI dynamics across diverse environmental backgrounds.

Exploring the spatiotemporal characteristics of surface UHI from a climate zone perspective is crucial [53]. Each climate zone may exhibit unique patterns of SUHII variation. Overall, our findings showed that tropical and subtropical cities (NSZ, MSZ, and SSZ) had significantly lower SUHII values than temperate cities (MTZ and STZ), particularly those in drier, higher-latitude areas, contrasting with the results of previous studies. For example, Peng et al. (2019) [54] explored large-scale spatiotemporal UHI patterns for 155 Chinese cities from 1984 to 2013 and reported high annual air UHI intensities in arid and high-latitude areas. Similarly, Zhang et al. (2011) [55] found that, during summer, cities in the NSZ, MSZ, and SSZ were particularly influenced by monsoons and ocean currents, and experienced more rapid urbanization, land surface changes, and increased heat emissions than temperate cities, suggesting higher SUHII. However, our results are consistent with the findings of other studies that examined the small-scale contribution of local climate zones in five climate regions [56].

Examining the long-term spatiotemporal variation in the SUHII is a key step in mitigating the UHI effect. We conducted Mann–Kendall tests to analyze and statistically verify the observed upward trend in the SUHII since the beginning of the 21st century. Numerous studies have documented trends in the summer daytime SUHII across cities in China, Brazil, and other countries. In Brazil, 61.90% of diurnal UHI effects in 21 metropolitan areas exhibited a significant upward trend [57]. Similarly, in China more than 80% of 302 cities experienced an increase in SUHII between 2003 and 2016, with approximately half of these trends being significant ($p < 0.05$) [49]. When considering only major Chinese cities, 75.90% showed a significant upward trend in SUHII ($p < 0.05$). The percentage of cities with significant increasing or decreasing summer daytime SUHII trends in the NSZ,

MSZ, and SSZ was higher than that in the MTZ and STZ, suggesting that each climate zone has a unique mechanism driving the UHI effect. Thus, tailored measures are needed to mitigate the UHI effect [21,25]. The high number of cities with significant increasing trends in summer daytime SUHII suggests that further adaptation strategies to address the UHI effect during this season are urgently required.

4.2. Effect of SUHII-Influencing Factors in Different Climate Zones

The mechanisms underlying the UHI effect exhibit spatiotemporal variability and heterogeneity across different climates [14,25,43]. In this study, biophysical characteristics and SUHII had significant effects on all climate zones except the STZ. AOD and PRE—which are primarily governed by natural factors—were the primary influencing factors, jointly accounting for more than 40.11%. EVI and urbanization also had significant effects: EVI contributed 48.78% and 14.19% to SUHII in the MTZ and SSZ, respectively, which urbanization contributed 18.54% and 25.96% in the MTZ and SSZ, respectively. Taken together, these findings indicate that the biophysical characteristics significantly influence the UHI effect [36,47]. Our findings are consistent with those of Pakarnseree et al. (2018) [58], who reported that the physical characteristics of Bangkok and its surrounding areas significantly affected UHI magnitude. Another study reported a significant positive correlation between the annual daytime SUHII and urban areas in Europe [43], which is somewhat consistent with our findings. However, some research has suggested that increased urban greening does not necessarily lead to lower surface temperatures, which contradicts our conclusions and necessitates further in-depth research [59].

Natural factors have a pronounced effect on cities within the STZ which are characterized by complex terrain and strong monsoonal effects. Many studies have explored AOD and PRE as key natural factors affecting the UHI effect. Aerosol and smog pollution are potential influencing factors in this regard. High aerosol concentrations reduce incoming solar radiation while increasing atmospheric longwave radiation, thereby influencing the UHI effect [60]. Compared to humid arid areas, semiarid areas experience a stronger UHI effect resulting from haze [61].

Socioeconomic factors, such as NL, POP, and GDP, reflect the impact of human activity on the UHI effect. In our study, these factors affected cities in all climate zones, with notable impacts in the MTZ, STZ, and NSZ, although no significant correlations were identified. Sultana and Satyanarayana (2018) [62] reported that while socioeconomic may variables have limited direct impacts on SUHII, they often indirectly influence the intensity of the UHI effect by altering the physical environment. Yuan et al. (2022) [26] argued that global SUHII is influenced by a combination of factors rather than a single dominant factor. The key factors affecting the daytime SUHII were monthly precipitation and POP, followed by other factors. POP influences UHI through anthropogenic heat release, and our results are consistent with Chapman et al. (2016) [63], who identified anthropogenic heat as a major factor affecting UHIs in four Australian cities. Finally, GDP reflects industrial development, which may influence both natural factors such as AOD and biophysical characteristics such as EVA.

While multiple studies have explored various factors influencing the UHI effect, discrepancies persist, likely due to differences in how UHIs are defined, the selection of potential factors, and the timespans considered [44,45]. Our results indicated that the mechanisms underlying the UHI effect exhibit both temporal and climatic heterogeneity, enhancing our understanding of UHI evolution.

4.3. Implications and Limitations

The intensification of SUHII has multiple adverse consequences, including the aggravation of urban heatwaves, elevated energy demand, and the deterioration of public health and air quality. Our findings suggest that climate zones strongly modulate the influence of biophysical and socioeconomic drivers in shaping SUHII, offering valuable insights for climate-sensitive urban design. In the temperate zones (MTZ, STZ), where SUHII values and upward trends were most pronounced, vegetation coverage (EVI) and urban form were the primary determinants. This finding implies that urban greening—such as increasing canopy cover, implementing rooftop gardens, and restoring urban wetlands—can be highly effective [64,65]. In contrast, in the subtropical zones (NSZ, MSZ), socioeconomic factors such as GDP and population size had greater relative influence, highlighting the need for sustainable urban densification, industrial structure optimization, and energy-efficient development. Furthermore, in the STZ regions with complex terrain and haze-prone conditions, aerosols (AOD) were found to significantly affect SUHII, likely through altered radiation budgets. Policies targeting air pollution control (e.g., reducing fine particulate emissions and promoting electric transport) may yield co-benefits for both air quality and thermal comfort. The results align with recent district-based UHI mitigation studies such as that of Aslani et al. (2025) [24], who used machine learning models in Tehran to demonstrated the impacts of AOD, population density, and vegetation loss on UHI, providing a quantitative foundations for localized mitigation actions.

It should be noted that this study had some limitations. First, we relied on MODIS satellite data, which, despite offering high spatiotemporal resolution, are limited by source. Therefore, future studies should integrate other sources of remote sensing data and ground-based observations to improve the comprehensiveness and accuracy of the obtained results. Second, although we focused on the spatiotemporal characteristics and drivers of the UHI effect, we did not examine the integrated or synergistic effects of other environmental problems such as air and noise pollution. Therefore, further research on urban latent and sensible heat flux variations is required. Third, while we conducted Pearson's correlation and stepwise multiple regression analyses for the years 2001, 2005, 2010, 2015, and 2018, further detailed deep learning analyses involving data collected from 2000 to 2020 may have yielded stronger results.

5. Conclusions

To quantify the spatiotemporal characteristics and driving factors of UHI effects across different climate zones using long-term time-series data, we examined the spatiotemporal characteristics of the trends and potential factors influencing daytime SUHII in major Chinese cities in different climate zones from 2000 to 2020, using Mann–Kendall tests, Pearson's correlation, and multiple stepwise regression analyses. Our results showed that the average summer daytime SUHII varied significantly by climate zone, ranging from 1.75 °C (MTZ) to 2.37 °C (NSZ). A significant upward trend in SUHII was observed in 75.9% of cities, indicating widespread intensification of urban thermal stress. High-SUHII clusters were concentrated in the Yangtze River Basin and North China Plain. In major Chinese cities, the summer daytime SUHII values result from a combination of factors. Most climate zones are significantly influenced by both biophysical characteristics and socioeconomic factors, the latter of which alter the urban physical environment and indirectly affect SUHII, thereby necessitating targeted mitigation strategies. These findings emphasize the importance of climate-zone-sensitive UHI assessments and urban planning strategies. Overall, our findings provide a valuable reference for mitigating the UHI effect and reducing the frequency of weather events in specific climatic zones. By managing and

regulating relevant influencing factors, urban planners and policymakers can promote the sustainable development of human–environment-coupled systems.

Supplementary Materials: The following supporting information can be downloaded at https://www.mdpi.com/article/10.3390/ijgi14070239/s1. Figure S1: the climatic regionalization of China that established by China Meteorological Administration, including north temperate zone (NTZ), middle temperate zone (MTZ), south temperate zone (STZ), north subtropical zone (NSZ), middle subtropical zone (MSZ), south subtropical zone (SSZ) and north tropical zone (NRZ), middle tropical zone (MRZ), south tropical zone (SRZ) and Plateau climatic zone (PCZ).

Author Contributions: Minxue Zheng collected and analyzed the data and wrote the manuscript. Dianwei Zheng collected and processed the data. Qiu Shen analyzed the data. Feng Jia edited the manuscript and provided constructive comments. All authors have read and agreed to the published version of the manuscript.

Funding: This research received no external funding.

Data Availability Statement: The data that support the findings of this study are available as follows: the enhanced vegetation index (MODIS MOD13A2 products; 1000 m and 16 days), the landscape shape index, the percentage of ecological landscape, the percentage of water area, the percentage of forest area, the percentage of impervious surface, the percentage of cropland, the percentage of ecological proportion and cropland (land cover date from Chinese Academy of Sciences) (https://www.resdc.cn/Default.aspx (accessed on 21 June 2024)), city area [41], evapotranspiration [66], aerosol optical depth [67], elevation (ASTER GDEM; 30 m), net radiation [68], precipitation (Gong et al., 2022), 2022, gross domestic product, population density (Chinese Academy of Sciences), and nighttime light [69].

Conflicts of Interest: The authors declare no conflicts of interest.

References

1. Oke, T.R. The energetic basis of the urban heat island. *Q. J. R. Meteorol. Soc.* **1982**, *108*, 1–24. [CrossRef]
2. Ji, Q.; Bao, Y.; Wang, T.; Wu, J.; Chen, C. Study on the characteristics of urban heat island effect and its key influencing factors in Kunshan. *Sci. Meteorol. Sin.* **2023**, *43*, 155–166. [CrossRef]
3. Li, Y.; Schubert, S.; Kropp, J.P.; Rybski, D. On the influence of density and morphology on the Urban Heat Island intensity. *Nat. Commun.* **2020**, *11*, 2647. [CrossRef] [PubMed]
4. Stewart, I.D.; Krayenhoff, E.S.; Voogt, J.A.; Lachapelle, J.A.; Allen, M.A.; Broadbent, A.M. Time Evolution of the Surface Urban Heat Island. *Earth's Future* **2021**, *9*, e2021EF002178. [CrossRef]
5. Matthews, T.; Ramsay, E.E.; Saeed, F.; Sherwood, S.; Jay, O.; Raymond, C.; Abram, N.; Lee, J.K.W.; Barley, S.; Perkins-Kirkpatrick, S.; et al. Humid Heat Exceeds Human Tolerance Limits and Causes Mass Mortality. *Nat. Clim.* **2025**, *15*, 4–6. [CrossRef]
6. Li, D.; Bou-Zeid, E. Synergistic Interactions between Urban Heat Islands and Heat Waves: The Impact in Cities Is Larger than the Sum of Its Parts. *J. Appl. Meteorol. Clim.* **2013**, *52*, 2051–2064. [CrossRef]
7. Canton, J.; Dipankar, A. Climatological analysis of urban heat island effects in Swiss cities. *Int. J. Clim.* **2024**, *44*, 1549–1565. [CrossRef]
8. Yao, R.; Wang, L.; Huang, X.; Niu, Z.; Liu, F.; Wang, Q. Temporal trends of surface urban heat islands and associated determinants in major Chinese cities. *Sci. Total Environ.* **2017**, *609*, 742–754. [CrossRef]
9. Imhoff, M.L.; Zhang, P.; Wolfe, R.E.; Bounoua, L. Remote sensing of the urban heat island effect across biomes in the continental USA. *Remote Sens. Environ.* **2010**, *114*, 504–513. [CrossRef]
10. Parmeggiani, D.; Despini, F.; Costanzini, S.; Silvestri, M.; Rabuffi, F.; Teggi, S.; Ghermandi, G. Assessing Satellite Data's Role in Substituting Ground Measurements for Urban Surfaces Characterization: A Step towards UHI Mitigation. *Atmosphere* **2024**, *15*, 551. [CrossRef]
11. Nayak, S.; Vinod, A.; Prasad, A.K. Spatial Characteristics and Temporal Trend of Urban Heat Island Effect over Major Cities in India Using Long-Term Space-Based MODIS Land Surface Temperature Observations (2000–2023). *Appl. Sci.* **2023**, *13*, 13323. [CrossRef]
12. Yao, R.; Wang, L.; Huang, X.; Zhang, W.; Li, J.; Niu, Z. Interannual variations in surface urban heat island intensity and associated drivers in China. *J. Environ. Manag.* **2018**, *222*, 86–94. [CrossRef] [PubMed]
13. Ramamurthy, P.; Bou-Zeid, E. Heatwaves and urban heat islands: A comparative analysis of multiple cities. *J. Geophys. Res. Atmos.* **2016**, *122*, 168–178. [CrossRef]

14. Manoli, G.; Fatichi, S.; Schläpfer, M.; Yu, K.; Crowther, T.; Meili, N.; Burlando, P.; Katul, G.G.; Bou-Zeid, E. Magnitude of urban heat islands largely explained by climate and population. *Nature* **2019**, *573*, 55–60. [CrossRef]
15. Marquès, E.; Masson, V.; Naveau, P.; Mestre, O.; Dubreuil, V.; Richard, Y. Urban Heat Island Estimation from Crowdsensing Thermometers Embedded in Personal Cars. *Bull. Am. Meteorol. Soc.* **2022**, *103*, E1098–E1113. [CrossRef]
16. Tetali, S.; Baird, N.; Klima, K. A multicity analysis of daytime surface urban heat islands in India and the US. *Sustain. Cities Soc.* **2022**, *77*, 103568. [CrossRef]
17. Di, J.; Su, T.; Lei, B.; Liu, X.; Meng, C.; Xu, L.; Wang, R. Analysis of urban heat island effect and influencing factors based on the "source-sink" landscape pattern: A case study of Hefei. *China Environ. Sci.* **2023**, *43*, 6039–6050. [CrossRef]
18. Rini, E.F. Spatial Pattern of Urban Heat Island to Enhance Urban Cooling Ecosystem Services in the Post-Pandemic Era. *IOP Conf. Ser. Earth Environ. Sci.* **2023**, *1264*, 012044. [CrossRef]
19. Qin, M.; Ouyang, H.; Jiang, H.; Luo, T.; Zhou, Y.; Liu, Y. Spatiotemporal evolution characteristics and driving factors of heat island effect based on territorial perspective: A case study of Beibu Gulf urban agglomeration, China. *Ecol. Indic.* **2024**, *166*, 112197. [CrossRef]
20. Mehmood, M.S.; Rehman, A.; Sajjad, M.; Song, J.; Zafar, Z.; Shiyan, Z.; Yaochen, Q. Evaluating land use/cover change associations with urban surface temperature via machine learning and spatial modeling: Past trends and future simulations in Dera Ghazi Khan, Pakistan. *Front. Ecol. Evol.* **2023**, *11*, 1115074. [CrossRef]
21. Zou, Z.; Yan, C.; Yu, L.; Jiang, X.; Ding, J.; Qin, L.; Wang, B.; Qiu, G. Impacts of land use/ land cover types on interactions between urban heat island effects and heat waves. *Build. Environ.* **2021**, *204*, 108138. [CrossRef]
22. Jin, K.; Wang, F.; Wang, S. Assessing the spatiotemporal variation in anthropogenic heat and its impact on the surface thermal environment over global land areas. *Sustain. Cities Soc.* **2020**, *63*, 102488. [CrossRef]
23. Lu, Y. The Mechanism of Urban Form Affecting Heat Island Effect. In *Urban Form and Urban Heat Island: Towards a Cool Built Environment*; Lu, Y., Ed.; Springer Nature Singapore: Singapore, 2025; pp. 121–160.
24. Aslani, A.; Sereshti, M.; Sharifi, A. Urban heat island mitigation in Tehran: District-based mapping and analysis of key drivers. *Sustain. Cities Soc.* **2025**, *125*, 106338. [CrossRef]
25. Zhao, L.; Lee, X.; Smith, R.; Oleson, K. Strong contributions of local background climate to urban heat islands. *Nature* **2014**, *511*, 216–219. [CrossRef]
26. Yuan, Y.; Li, C.; Geng, X.; Yu, Z.; Fan, Z.; Wang, X. Natural-anthropogenic environment interactively causes the surface urban heat island intensity variations in global climate zones. *Environ. Int.* **2022**, *170*, 107574. [CrossRef]
27. Lefevre, A.; Malet-Damour, B.; Bénard, F.; Boyer, H.; Rivière, G. Integrating urban heat island analysis for sustainable urban planning: Insights from Reunion Island. *Build. Environ.* **2025**, *278*, 112964. [CrossRef]
28. Wang, Y.; Sun, R. Impacts of regional climate on heat islands in China. *Acta Ecol. Sin.* **2021**, *41*, 4288–4299.
29. Kim, H.; Gu, D.; Kim, H.Y. Effects of Urban Heat Island mitigation in various climate zones in the United States. *Sustain. Cities Soc.* **2018**, *41*, 841–852. [CrossRef]
30. Mohammad, P.; Goswami, A. Quantifying diurnal and seasonal variation of surface urban heat island intensity and its associated determinants across different climatic zones over Indian cities. *GISci. Remote Sens.* **2021**, *58*, 955–981. [CrossRef]
31. Fricke, C.; Pongrácz, R.; Gál, T.; Savić, S.; Unger, J. Using local climate zones to compare remotely sensed surface temperatures in temperate cities and hot desert cities. *Morav. Geogr. Rep.* **2020**, *28*, 48–60. [CrossRef]
32. Li, K.; Chen, Y.; Gao, S. Uncertainty of city-based urban heat island intensity across 1112 global cities: Background reference and cloud coverage. *Remote Sens. Environ.* **2022**, *271*, 112898. [CrossRef]
33. Zheng, J.; Yin, Y. A New Scheme for Climate Regionalization in China. *Acta Geogr. Sin.* **2010**, *65*, 3–12.
34. Wan, Z. New refinements and validation of the collection-6 MODIS land-surface temperature/emissivity product. *Remote Sens. Environ.* **2014**, *140*, 36–45. [CrossRef]
35. Yao, R.; Wang, L.; Huang, X.; Liu, Y.; Niu, Z.; Wang, S.; Wang, L. Long-term trends of surface and canopy layer urban heat island intensity in 272 cities in the mainland of China. *Sci. Total Environ.* **2021**, *772*, 145607. [CrossRef]
36. Feng, R.; Wang, F.; Wang, K.; Wang, H.; Li, L. Urban ecological land and natural-anthropogenic environment interactively drive surface urban heat island: An urban agglomeration-level study in China. *Environ. Int.* **2021**, *157*, 106857. [CrossRef]
37. Ren, T.; Zhou, W.; Wang, J. Beyond intensity of urban heat island effect: A continental scale analysis on land surface temperature in major Chinese cities. *Sci. Total Environ.* **2021**, *791*, 148334. [CrossRef]
38. Su, H.; Han, G.; Li, L.; Qin, H. The impact of macro-scale urban form on land surface temperature: An empirical study based on climate zone, urban size and industrial structure in China. *Sustain. Cities Soc.* **2021**, *74*, 103217. [CrossRef]
39. Voogt, J.A.; Oke, T.R. Thermal remote sensing of urban climates. *Remote Sens. Environ.* **2003**, *86*, 370–384. [CrossRef]
40. Meng, Q.; Zhang, L.; Sun, Z.; Meng, F.; Wang, L.; Sun, Y. Characterizing spatial and temporal trends of surface urban heat island effect in an urban main built-up area: A 12-year case study in Beijing, China. *Remote Sens. Environ.* **2018**, *204*, 826–837. [CrossRef]
41. Zhao, M.; Cheng, C.; Zhou, Y.; Li, X.; Shen, S.; Song, C. A global dataset of annual urban extents (1992–2020) from harmonized nighttime lights. *Earth Syst. Sci. Data* **2022**, *14*, 517–534. [CrossRef]

42. Demuzere, M.; Kittner, J.; Martilli, A.; Mills, G.; Moede, C.; Stewart, I.D.; van Vliet, J.; Bechtel, B. A global map of local climate zones to support earth system modelling and urban-scale environmental science. *Earth Syst. Sci. Data* **2022**, *14*, 3835–3873. [CrossRef]
43. Peng, S.; Piao, S.; Ciais, P.; Friedlingstein, P.; Ottle, C.; Bréon, F.M.; Nan, H.; Zhou, L.; Myneni, R. Surface urban heat island across 419 global big cities. *Environ. Sci. Technol.* **2012**, *46*, 696–703. [CrossRef] [PubMed]
44. Kim, S.W.; Brown, R.D. Urban heat island (UHI) variations within a city boundary: A systematic literature review. *Renew. Sustain. Energ. Rev.* **2021**, *148*, 1–18. [CrossRef]
45. Nina, S.; Sven, L.; Ralf, S. Exploring indicators for quantifying surface urban heat islands of European cities with MODIS land surface temperatures. *Remote Sens. Environ.* **2011**, *115*, 3175–3186.
46. Clinton, N.; Gong, P. MODIS detected surface urban heat islands and sinks: Global locations and controls. *Remote Sens. Environ.* **2013**, *134*, 294–304. [CrossRef]
47. Oukawa, G.Y.; Krecl, P.; Targino, A.C. Fine-scale modeling of the urban heat island: A comparison of multiple linear regression and random forest approaches. *Sci. Total Environ.* **2022**, *815*, 152836. [CrossRef]
48. Li, D.; Liao, W.; Rigden, A.; Liu, X.; Wang, D.; Malyshev, S.; Shevliakova, E. Urban heat island: Aerodynamics or imperviousness? *Sci. Adv.* **2019**, *5*, eaau4299. [CrossRef]
49. Yang, Q.; Huang, X.; Tang, Q. The footprint of urban heat island effect in 302 Chinese cities: Temporal trends and associated factors. *Sci. Total Environ.* **2019**, *655*, 652–662. [CrossRef]
50. Sun, R.; Lü, Y.; Yang, X.; Chen, L. Understanding the variability of urban heat islands from local background climate and urbanization. *J. Clean. Prod.* **2019**, *208*, 743–752. [CrossRef]
51. Montaner-Fernández, D.; Morales-Salinas, L.; Rodriguez, J.S.; Cárdenas-Jirón, L.; Huete, A.; Fuentes-Jaque, G.; Pérez-Martínez, W.; Cabezas, J. Spatio-Temporal Variation of the Urban Heat Island in Santiago, Chile during Summers 2005–2017. *Remote Sens.* **2020**, *12*, 3345. [CrossRef]
52. Li, X.; Asrar, G.; Imhoff, M.; Li, X. The surface urban heat island response to urban expansion: A panel analysis for the conterminous United States. *Sci. Total Environ.* **2017**, *605*, 426–435. [CrossRef] [PubMed]
53. Amorim, M.C.d.C.T.; Dubreuil, V.; Amorim, A.T. Day and night surface and atmospheric heat islands in a continental and temperate tropical environment. *Urban Clim.* **2021**, *38*, 1–15. [CrossRef]
54. Peng, S.; Feng, Z.; Liao, H.; Huang, B.; Peng, S.; Zhou, T. Spatial-temporal pattern of, and driving forces for, urban heat island in China. *Ecol. Indic.* **2019**, *2019*, 127–132. [CrossRef]
55. Zhang, J.; Chang, L.; Sone, Y.; Silber, S. Erratum to "Minimal ovarian stimulation (mini-IVF) for IVF utilizing vitrification and cryopreserved embryo transfer" [Reprod. Biomed. Online 21 (2010) 485–495]. *Reprod. Biomed. Online* **2011**, *23*, 396. [CrossRef]
56. Yu, Z.; Yao, Y.; Yang, G.; Wang, X.; Vejre, H. Spatiotemporal patterns and characteristics of remotely sensed region heat islands during the rapid urbanization (1995–2015) of Southern China. *Sci. Total Environ.* **2019**, *674*, 242–254. [CrossRef]
57. Monteiro, F.F.; Gonçalves, W.A.; Andrade, L.; Villavicencio, L.M.M.; dos Santos Silva, C.M. Assessment of Urban Heat Islands in Brazil based on MODIS remote sensing data. *Urban Clim.* **2021**, *35*, 100726. [CrossRef]
58. Pakarnseree, R.; Chunkao, K.; Bualert, S. Physical characteristics of Bangkok and its urban heat island phenomenon. *Build. Environ.* **2018**, *143*, 561–569. [CrossRef]
59. Wang, J.; Zhou, W. More urban greenspace, lower temperature? Moving beyond net change in greenspace. *Agric. For. Meteorol.* **2022**, *322*, 109021. [CrossRef]
60. Kasimov, N.; Chalov, S.; Chubarova, N. Urban heat and pollution island in the Moscow megacity: Urban environmental compartments and their interactions. *Urban Clim.* **2024**, *55*, 101972. [CrossRef]
61. Cao, C.; Lee, X.; Liu, S.; Schultz, N.; Xiao, W.; Zhang, M.; Zhao, L. Urban heat islands in China enhanced by haze pollution. *Nat. Commun.* **2016**, *7*, 12509. [CrossRef]
62. Sultana, S.; Satyanarayana, A.N.V. Urban heat island intensity during winter over metropolitan cities of India using remote-sensing techniques: Impact of urbanization. *Int. J. Remote Sens.* **2018**, *39*, 6692–6730. [CrossRef]
63. Chapman, S.; Watson, J.E.M.; McAlpine, C.A. Large seasonal and diurnal anthropogenic heat flux across four Australian cities. *J. South. Hemisph. Earth Syst. Sci.* **2016**, *31*, 1990–2005.
64. Wang, J.; Zhou, W.; Pickett, S.T.A.; Qian, Y. A scaling law for predicting urban trees canopy cooling efficiency. *Proc. Natl. Acad. Sci. USA* **2024**, *121*, e2401210121. [CrossRef] [PubMed]
65. Yu, Z.; Chen, J.; Chen, J.; Zhan, W.; Wang, C.; Ma, W.; Yao, X.; Zhou, S.; Zhu, K.; Sun, R. Enhanced observations from an optimized soil-canopy-photosynthesis and energy flux model revealed evapotranspiration-shading cooling dynamics of urban vegetation during extreme heat. *Remote Sens. Environ.* **2024**, *305*, 114098. [CrossRef]
66. Cheng, M.; Jiao, X.; Li, B.; Yu, X.; Shao, M.; Jin, X. Long time series of daily evapotranspiration in China based on the SEBAL model and multisource images and validation. *Earth Syst. Sci. Data* **2021**, *13*, 3995–4017. [CrossRef]

67. Bai, K.; Li, K.; Ma, M.; Li, K.; Li, Z.; Guo, J.; Chang, N.B.; Tan, Z.; Han, D. LGHAP: The Long-term Gap-free High-resolution Air Pollutant concentration dataset, derived via tensor-flow-based multimodal data fusion. *Earth Syst. Sci. Data* **2022**, *14*, 907–927. [CrossRef]
68. Xu, J.; Liang, S.; Jiang, B. A global long-term (1981–2019) daily land surface radiation budget product from AVHRR satellite data using a residual convolutional neural network. *Earth Syst. Sci. Data* **2022**, *14*, 2315–2341. [CrossRef]
69. Chen, Z.; Yu, B.; Yang, C.; Zhou, Y.; Yao, S.; Qian, X.; Wang, C.; Wu, B.; Wu, J. An extended time series (2000–2018) of global NPP-VIIRS-like nighttime light data from a cross-sensor calibration. *Earth Syst. Sci. Data* **2021**, *13*, 889–906. [CrossRef]

Disclaimer/Publisher's Note: The statements, opinions and data contained in all publications are solely those of the individual author(s) and contributor(s) and not of MDPI and/or the editor(s). MDPI and/or the editor(s) disclaim responsibility for any injury to people or property resulting from any ideas, methods, instructions or products referred to in the content.